Faraday Discussions

Predicting third-body collision efficiencies for water and other polyatomic baths

Journal:	*Faraday Discussions*
Manuscript ID	FD-ART-02-2022-000038.R1
Article Type:	Paper
Date Submitted by the Author:	07-Mar-2022
Complete List of Authors:	Jasper, Ahren; Argonne National Laboratory,

Predicting third-body collision efficiencies for water and other polyatomic baths

Ahren W. Jasper

Chemical Sciences and Engineering Division, Argonne National Laboratory, Lemont, Illinois 60439, USA

Low-pressure-limit microcanonical (collisional activation) and thermal rate constants are predicted using a combination of automated ab initio potential energy surface construction, classical trajectories, transition state theory, and a detailed energy- and angular-momentum-resolved collision kernel. Several systems are considered, including CH_4 (+M) and HO_2 (+M), with an emphasis on systems where experimental information is available for comparison. The a priori approach involves no adjustable parameters, and we show that the predicted thermal rate constants are in excellent agreement with experiment, with average deviations of less than 25%. Notably, the a priori approach is shown to perform equally well for atomic, diatomic, and polyatomic baths, including M = H_2O, CO_2, and "fuel" baths like M = CH_4 and NH_3. Finally, the utility of microcanonical rate constants for interpreting trends and inferring mechanistic details in the thermal kinetics is demonstrated.

I. Introduction

The Lindemann–Hinshelwood expression[1,2] for the pressure-dependent rate constant k_p of a unimolecular reaction A (+M) $\rightarrow$ A* (+M) $\rightarrow$ B + C is obtained by imposing a steady state condition on the concentration of the energized reactant A* and explains the apparent change in the order of k_p from second to first with increasing pressure p. Although not written this way 100 years ago, the expression can be rearranged to

$$\frac{1}{k_p} = \frac{1}{k_0 n_M} + \frac{1}{k_\infty}, \quad (1)$$

where the second-order collisional activation rate constant k_0 is multiplied by the number density n_M of the "third-body" M such that $k_0 n_M$ depends linearly on pressure, and k_∞ is the first-order intramolecular dissociation rate constant and is independent of pressure. Eqn 1 can be used to describe both microcanonical (here, total-energy- and total-angular-momentum-resolved) unimolecular rate constants $k_p(E,J)$ as well as thermal unimolecular rate constants $k_p(T)$, including the RRK and RRKM expressions[3–6] with appropriate choices for k_0 and k_∞.

The form of eqn 1 emphasizes that unimolecular reactivity results from the competition of two dynamical bottlenecks: one is associated with collisional activation and is dominant at low pressures, and another is associated with intramolecular energy rearrangements and bond breaking and is dominant at high pressures. Despite their apparent symmetry in eqn 1, considerably more effort in the past 100 years has gone into developing a priori theoretical methods for predicting k_∞ than k_0.

High pressure limit rate constants k_∞ are conveniently and often accurately predicted using ab initio transition state theory (TST).[6–10] Ab initio TST has been repeatedly validated against higher-level theories as well as experiment, and continuing efforts are being made to understand

its general accuracy and limitations. Just as importantly, a useful chemical intuition regarding the connection between transition state structures and chemical mechanisms has been developed.

In contrast, k_0 is only rarely predicted. Pressure dependence, when it is not ignored, is instead typically treated using empirical models containing a few adjustable parameters. The parameters are either estimated or tuned to match the model's predictions to measured values of k_p, if available. Experimental studies characterizing collision information,[11–21] including measurements of the average energy transferred by collisions ΔE, have been important to our understanding of pressure dependent kinetics. When ΔE or equivalent experimental information is used to parametrize theoretical models, however, the results are not generally expected to be predictive, as the necessarily simple theoretical models are not sufficiently detailed. Furthermore, the lack of detailed predictive theories has left us with confounding observed trends in relative collision efficiencies (i.e., in relative values of $k_0(T)$) and prevented the development of a useful chemical intuition regarding the dependence of collision efficiencies and k_0 on temperature and the identity of the bath gas.

The goal of this work is to demonstrate accurate predictions for k_0 and k_p for polyatomic baths and to provide some discussion toward developing a chemical intuition for collisional activation. We consider falloff and low-pressure limit kinetics for several systems, focusing on the collision efficiency of water and other polyatomic baths relative to weaker common baths like N_2 and Ar. We consider thermal rate constants, which are compared with available experimental kinetics and collision efficiency measurements to further validate the a priori theory, as well as less-often considered microcanonical rate constants, which are briefly examined here for mechanistic insights.

II. Theory

Background. The thermal rate constant for a unimolecular reaction can be written as a weighted sum of microcanonical rate constants

$$k_p(T) = \sum_{J=0}^{\infty} \int_{E=0}^{\infty} dE\, k_p(E,J) x_p(E,J), \tag{2}$$

where E and J are the total energy and total angular momentum of the reactant, respectively, the arguments of k_p distinguish thermal and microcanonical rate constants, and the weights x_p are the population densities of the internal states of the reactant. In general, both $k_p(E,J)$ and $x_p(E,J)$ are functions of the temperature T as well as the identity of the bath gas M, but this dependence is not noted to avoid clutter. Only in the high pressure limit, where $k_\infty(E,J) = N^\ddagger/h\rho$ and $x_\infty = \rho \exp(-E/k_B T)/Q$ have familiar expressions from Marcus[5] and Boltzmann, respectively, are the kinetics independent of the identity of the bath gas M. If we wish to characterize falloff and low-pressure–limit kinetics, $k_0(E,J)$ and $x_0(E,J)$ must be predicted separately for each temperature and bath gas of interest.

In the low-pressure-limit, microcanonical rate constants describe the rate of activating collisions and have the form[22,23]

$$k_0(E,J) = \sum_{J'=0}^{\infty} \int_{E_{J'}}^{\infty} dE'\, R(E',J';E,J), \qquad \text{for } E < E_J, \tag{3}$$

where E_J is the J-dependent dissociation threshold for the reactant, and $k_0(E,J)$ is not defined for unbound initial states. The integrand of eqn 3, R, is sometimes called the "collision kernel" and describes the rate at which collisions knock the reactant from the initial state (E,J) to the final state (E',J'); the limits in eqn 3 ensure that $k_0(E,J)$ counts only those collisions that knock the system

from a bound state to an unbound one. Again, R depends on T and M, but this dependence is not noted.

The state-to-state collisional transfer rate constant R and its low-order moments have been characterized many times using ensembles of classical trajectories (see, for example,[24–38] as well as own studies[39–43]), with a particularly useful characterization of R given by Barker and Weston;[44] this extensive literature was recently reviewed and interpreted by Lendvay.[45] In general, the trajectory studies connect observed properties of R to mechanistic details of the collisions, including a nonexponential dependence on the energy transferred $\Delta E = |E' - E|$ with a long tail associated with so-called "supercollisions," nonseparability of energy and angular momentum transfer, and a strong dependence of R on the initial rotational state J with a relatively weaker dependence on E.

The state-to-state collisional transfer rate constant R is often written as the product of a bimolecular (reactant + bath) total collision rate constant, Z, and a normalized probability for collision outcomes, $P = R/Z$. This same substitution lets us write eqn 3 as

$$k_0(E,J) = Z\,F(E,J) \tag{4}$$

where

$$F(E,J) = \sum_{J'} \int_{E_{J'}}^{\infty} dE\, P(E',J';E,J) \tag{5}$$

is the fraction of reactant + bath collisions that activate the reactant above its dissociation threshold.

Trajectories. We recently showed that $k_0(E,J)$ and F can be computed straightforwardly using classical trajectories,[23] and that the trajectory simulations can be automated.[43] We do not repeat many details here and instead provide an outline of the procedure with an emphasis on

considerations for treating polyatomic baths. Each simulation consists of an ensemble of trajectories defined by the initial state label (E,J) of the reactant A and the temperature T and the identity of the bath gas M. The internal coordinates of the reactant are determined subject to constraints imposed by the state label (E,J) by sampling from a small set of isolated trajectories for A(E,J).[40] Any internal coordinates of M and the relative A + M collision parameters are sampled classically using a thermostat and conventional bimolecular thermal sampling, respectively.[46,47] For each trajectory in the ensemble, the final total energy and angular momentum of A(E',J') are determined unambiguously once the reactant and bath had sufficiently separated. By comparing the final total energy E' to the dissociation threshold for the final rotational state J', $E_{J'}$, for all of the trajectories in the ensemble, the fraction of activation collisions F and in turn the desired microcanonical rate constants $k_0(E,J)$ are readily obtained.

Similar trajectory ensembles are used to compute ensemble-averaged changes in E and J due to collisions such as the well-known "average energy transferred in deactivating collisions" $\langle \Delta E_d \rangle$, along with other low-order moments of R. The "two-dimensional" master equation (2DME) kinetic model for R discussed below is parameterized against so-called "double moments," which are moments of R that include averaging over a distribution of initial states (E,J) along with final state averaging. We choose a thermal distribution for J and set E to a value close to the dissociation threshold of the reactant. Our best kinetic models are parametrized against all 135 double moments through third order,[57] and typical fitting errors of the moments are just ~15%, on average. Unlike in past work,[23] here we found that for some polyatomic colliders fitting the 45 second order moments resulted in predicted low-pressure limit kinetics that differed significantly from the third-order fits, by as much as 40%. This result reflects that k_0 is sensitive over a wider range of collision outcomes for stronger colliders than for weaker ones.

In the trajectory ensembles, the initial conditions, propagation, and final state assignments are all treated classically. This is done to ensure that average collisional energy and angular momentum transfer correctly tends to zero as the species thermalize. In other contexts, such as predicting reaction rate constants, it is often preferred to prepare the reactants quasiclassically,[48,49] where the internal states of the reactants are quantized prior to the collision event and the initial reactant energy therefore includes zero-point energy. This procedure inevitably leads to ambiguities with respect to final state assignments (which will not in general be quantized at the end of a classical simulation) with dramatic consequences often related to the treatment of zero-point-energy violations. Most importantly in the present context and in particular when dealing with polyatomic colliders, quasiclassical initial conditions cannot guarantee a tendency toward thermalized products, as the zero-point energies of the colliding species will tend toward equilibration along with the rest of the internal energy. We emphasize that the use of purely classical mechanics for characterizing collisional energy transfer is a choice, but it appears to be well supported by comparisons of our predictions with experimental kinetics, as demonstrated below.

Importantly, the dissociation thresholds E_J are *not* treated classically, and instead variational transition-state-theory-based thresholds are used. Classical mechanics is known to perform poorly near thresholds, and the present semiclassical prescription avoids this potentially significant source of error.

Total collision rates. It is often convenient to scale the microcanonical rate constants ($F = k_0/Z$) as well as the low-order moments of R such that the information they contain is written per-collision rather than per-time. The Lennard–Jones collision rate constants Z used here to do this are calculated using the "one-dimensional minimization" method.[50] It should be remembered that

our best kinetic models do not depend on this choice for *Z*. When any per-collision property appears in a detailed kinetics equation, it always appears multiplied by *Z* such that the arbitrary definition of a collision implied by the choice of *Z* does not affect the prediction.

Potential energy surfaces. For each system of interest, the interaction potential was described using permutationally invariant polynomial (PIP) expansions[51] parameterized and validated using a recently described automated strategy.[52,53] The PIP expansions were trained against large (>64,000) data sets of ab initio energies (typically, counterpoise corrected MP2 energies with complete basis set extrapolations). Convergence in the predicted energy transfer moments and rates with respect both to the order of the PIP expansion and the level of electronic structure theory used to train the PIPs was demonstrated previously.[52,53] Collision information is expected to be more sensitive to the interaction potential than to the intramolecular potential, and so the intramolecular PESs were described using a molecular mechanics force field with parameters confirmed or adjusted to predict experimental (NIST[54]) frequencies and rotational constants.

The flexibility provided by PIP expansions is important for accurately describing the complex and often highly anisotropic interaction potentials of the polyatomic baths considered here. We showed previously[52,53] that one could estimate relative errors in predicted collisional energy transfer moments due to fitting errors in the potential energy surface by computing a relative out-of-sample fitting error. For all the systems considered here, the order of the PIP expansion was chosen such that relative fitting errors were less than 20%. Simpler pairwise expressions for the interaction potential, such as the widely used Buckingham potential, cannot achieve this accuracy even for some diatomic baths.[52]

Thermal kinetics. To compute thermal rate constants, low-pressure-limit steady-state populations $x_0(E,J)$ are needed alongside $k_0(E,J)$. These were obtained by solving the two-dimensional master equation (2DME),[44,55–57] where the two dimensions are E and J. In the 2DME calculations, the collision kernel is described using a detailed model[57] designed to reproduce key collisional physics and trained against the trajectory-based "double moments" of R mentioned above. This model has no adjustable parameters and was previously shown to accurately predict thermal[57,58] and microcanonical[23] rate constants. Further demonstrations of the accuracy of this approach are given in the next section.

Predicting thermochemistry and high-pressure-limit rate constants is not the focus here, but these quantities are needed to fully characterized $k_p(T)$ and to compare with experiment. High-pressure limit kinetics $k_\infty(E,J)$ and dissociation thresholds E_J were calculated using Klippenstein's variable reaction coordinate TST (VRC-TST),[59,60] and anharmonic state densities and partition functions were calculated using semiclassical Monte Carlo phase space integrals[61,62] (MCPSI).

III. Results and Discussion

III.A. Thermal rate constants, relative collision efficiencies, and comparisons with experiment. First, we validate the a priori theoretical kinetics approach described above for predicting $k_p(T)$ at falloff pressures and $k_0(T)$ for a few systems where experimental information is available. We focus on predictions for polyatomic colliders.

Very similar theoretical approaches to the ones described here were previously used to predict $k_p(T)$ for CH_4 (+M) ⇌ CH_3 + H (+M), initially for He[57] and later for several atomic, diatomic, and polyatomic baths.[63] These calculations were repeated here using the automated PIP potential energy surface construction and trajectory strategies described above, and as expected

the new results are in close agreement with the earlier calculations (with moments of R typically differing by less than 10% from the earlier results). A new comparison with two sets of experimental results[64,65] around 1000 K for M = Ar and CH_4 is shown in Fig. 1. The predicted and measured rate constants typically differ by less than 25%, as indicated by 25% error bars added to the theoretical curves, and these deviations are consistent with earlier comparisons[57,58] and assessments.[23] There are somewhat larger deviations from the higher-pressure measurements for M = Ar, and the source of these deviations is unclear. The present predictions are in very close agreement with experiment at lower pressures where the rate constants are most sensitive to the description of collisional energy transfer, which is the focus of the present study.

Notably, at the lowest experimental pressures considered (~0.05 atm for M = CH_4), the experimental data could be interpreted as showing a near linear dependence with pressure, whereas the theoretical results show somewhat more curvature. This difference in interpretation can affect experimental determinations of k_0. For example, Fig. 2(a) shows predicted values of $k_p(T = 1000$ K) for CH_4 (+M) $\rightarrow$ CH_3 + H (+M) in five baths including three polyatomic baths (M = Ar, N_2, CO_2, CH_4, and H_2O), and their values relative to those for M = Ar are plotted in Fig. 2(b). Over the experimental pressure ranges from Fig. 1 (0.03 to 1 atm and 5 to 50 atm), the relative values of k_p deviate from those at lower pressures and therefore from the relative values of k_0 by as much as a factor of two to three.

In practice, low enough pressures required to accurately determine k_0 from experiment may be well outside the range of accessible pressures, and indeed these pressures might be too low to be relevant to any practical application. Even when the unimolecular kinetics of interest is close to the high-pressure limit, the magnitude of any pressure-dependent "falloff" is nonetheless controlled by collisional energy transfer and its competition with intramolecular kinetics. The

theoretical consideration of the effect of collisional energy transfer on kinetics is conveniently studied by considering k_0, and k_0 is the focus of the remainder of this article.

Figure 3 compares predicted low-pressure limit rate constants for H + O_2 + M, M = Ar, N_2, CO_2, and H_2O, around 1000 K with measurements reported in three experimental studies from Hanson and co-workers.[66–68] The calculated HO_2 (+M) → H + O_2 (+M) rate constants were reversed to match the reported experiments. Focusing on the most recent experimental study (Shao et al.[68] indicated in Fig. 3 by squares), we see that the predictions are in close agreement with the measured values and are typically within their assigned error bars of less than 15%. The Shao et al. study was conducted at pressures as low as 13 atm, and Fig. 3 shows that our calculated rate constants at 13 atm are ~10% lower than the LPL and appear in even better agreement with Shao et al. Notably, based on these comparisons, the present theoretical procedure appears to work equally well for the weaker colliders Ar and N_2 and the stronger colliders CO_2 and H_2O.

Table 1 summarizes calculated bath gas collision efficiencies (i.e., the relative values of k_0) for the systems discussed so far, CH_4 (+M) and HO_2 (+M), including some new baths and alongside results for additional systems where comparisons with experimental bath gas efficiencies can be made. A large number experimental studies have been carried out for some of the systems in Table 1, and we cannot attempt comprehensive comparisons here. Instead, we rely on recent experiments and evaluations given by others. We note that preliminary versions of these results for HO_2 (+M), H_2O_2 (+M), NH_3 (+M), and N_2H_4 (+M) were mentioned in an earlier paper describing the generation of their potential energy surfaces.[53] Here, these results are expanded and analyzed in more detail.

For HO_2 (+M), Michael et al.[69] measured (and reviewed existing) collision efficiencies at room temperature that are seen to be in good agreement with the present predictions, as shown in

Table 1. At higher temperatures, Ashman and Haynes[70] reported relative collision efficiencies from 750–900 K for M = Ar, N_2, CO_2, and H_2O, and the experimental study of Shao et al.[68] highlighted in Fig. 3 considered these same baths around ~1500 K. In Refs. 69 and 70, the measured rate constants were assigned uncertainties of ~30% or more (and if we assume that errors for different baths are uncorrelated the uncertainty in the ratios given in Table 1 would be √2-times larger). The calculated values typically agree within these experimental errors, although we find an exception in the factor of ~2 difference for HO_2 (+CO_2) at 1000 K. Agreement with the higher-temperature data set of Shao et al., which includes CO_2, is excellent as emphasized by Fig. 3. Notably, the theory correctly predicts the very large relative collision efficiency of water $k_0(H_2O)/k_0(Ar) > 20$, in agreement with experiment.[68,69]

For H_2O_2 (+M), we refer to a recent theoretical study by Matsugi[71] who used similar trajectory approaches but did not solve the 2DME. He provided a discussion of available experiments, most of which are older, and the discussion is not repeated here. Instead, Table 1 includes one comparison with a set of more recent experimental results[72] around 1000 K, where agreement is again seen to be good, though we note factor of ~2 differences for M = CO_2 and H_2O_2.

For H_2O (+M), M = Ar and H_2O, we compare our predicted results with experimentally informed expressions given by Srinivasan and Michael.[73] The recommended expressions show an increase in the relative rate constants for H_2O and Ar with temperature, whereas the predicted collision efficiencies show no temperature dependence. Quantitatively, the two values are nonetheless in fair agreement with one another, with deviations close to the experimentally assigned uncertainties.

A comparison of predicted and experimental collision efficiencies was recently made for NH_3 (+M) and N_2H_4 (+M) and for several baths including polyatomic colliders.[74] The results are summarized in Table 1. Although we are not aware of experimental measurements for NH_3 (+Ar), our current predicted relative values of N_2:CH_4:CO_2 = 1 : 3.15 : 3.54 for NH_3 (+M) at 300 K agree well with the relative experimental values of 1 : 2.60 : 2.83 of Macdonald and co-workers.[75–77] Similarly good agreement with experiment[75–78] is found for N_2H_4 (+M), as shown in Table 1. New results for M = H_2O have been added for NH_3(+M) and N_2H_4(+M). Finally, Table 1 includes a small set of results for HNO (+M) and HCN (+M) to add some variety.

The comparisons in Table 1 alongside more the detailed comparisons in Figs. 1 and 3 and elsewhere[23,57,58] suggest a predictive accuracy in our theoretical approach of better than ~25%. Sometimes larger deviations are observed in Table 1, but we note relatively large uncertainties in the experimental work. When precise and systematic data sets are available, relative efficiencies are predicted in excellent agreement with experiment, as demonstrated in Fig. 3 and elsewhere.[23,57,58] Importantly, collision efficiencies for polyatomic colliders are shown to be predicted just as accurately as those for weaker colliders. This demonstration is the major result of this work.

In the remainder of the paper, we look for trends in Table 1 and analyze a few cases in more detail. Qualitative trends in Table 1 support the following conventional assumptions often made about collision efficiencies.

N_2 is consistently a stronger collider than Ar, with $k_0(N_2)/k_0(Ar) \approx 1.5–3$, although a notable exception is CH_4 (+M), where $k_0(N_2)/k_0(Ar) \approx 1$. CH_4 (+M) is one of the more widely studied systems in this context, which could be the source of the occasional assumption that the two baths generally have similar efficiencies.

The atomic and diatomic baths (He, H_2, N_2, and O_2), typically considered "weak" colliders, are predicted to have collision efficiencies relative to Ar of around 1 to 3, whereas H_2O and polyatomic "fuel" baths (NH_3, CH_4, and H_2O_2) have much larger collision efficiencies relative to Ar of around 10–20. Unfortunately, there is significant dispersion in the results, with results for $k_0(H_2O)/k_0(Ar)$ varying from 4 to 28, for example, suggesting that universal bath gas efficiencies may not be suitable in many contexts.

Finally, relative collision efficiencies are often but are not always temperature dependent. The collision efficiency of CO_2 relative to Ar tends to decrease somewhat with temperature, while this trend is reversed for $k_0(H_2O)/k_0(Ar)$, but overall it appears difficult to generalize trends in the temperature dependence of $k_0(M)/k_0(Ar)$ with M. Collision efficiencies for some systems increase by as much as a factor of 2.5 from 300 to 2000 K and decrease by as much as a factor of 4.5 for other systems over this same temperature range.

III.B. Microcanonical rate constants. In a recent study,[23] we suggested that trends in relative thermal low-pressure-limit rate constants $k_0(T)$, i.e., in relative collision efficiencies, are confounded by a strong sensitivity of the underlying microcanonical low-pressure limit rate constants to the initial state (E,J). Microcanonical low-pressure limit rate constants $k_0(E,J)$ are discussed next for HO_2 (+M), M = Ar, N_2, CO_2, NH_3, and H_2O.

In Fig. 4, the integrand of eqn 2, $k_0(E,J)x_0(E,J)$, i.e., the initial-state-selected contribution to the thermal rate constant, is plotted for HO_2 (+M) at 1000 K for four baths. (M = NH_3 was also considered; its contour plot is similar to that for M = H_2O and is not shown.) The relative thermal collision efficiencies for these baths are $Ar:N_2:CO_2:NH_3:H_2O$ = 1 : 1.6 : 8.9 : 18 : 22, and indeed these relative efficiencies are reflected in the shapes of the contours in Fig. 4.

All four distributions peak around the same initial state (E = 600 cm^{-1}, J = 28 $\hbar$), with the location of this "preferred" initial state largely controlled by the variation in the density of states of the reactant $\rho(E_J,J)$ along the threshold for dissociation E_J. Strong and weak colliders deplete threshold states to different degrees, and it is notable that these differences do not shift the preferred state.

The contours in Fig. 4 are linearly spaced, and for the two weaker colliders the distributions are seen to decrease sharply with energy, with insignificant contributions to reactivity for states more than a ~500 cm^{-1} below threshold. Notably, the range of depletion is nearly independent of the initial rotational state J over a broad range of J, suggesting that one-dimensional kinetic models for treating J (i.e., models that ignore the nonseparability[44] of E and J) may be appropriate. The more rounded shapes for the stronger colliders, M = CO_2, NH_3, and H_2O, however, clearly reveal strong E and J coupling and indicate that explicitly two-dimensional master equation models are needed for quantitative descriptions. The qualitatively different initial-rotational-state preferences for strong and weak baths suggest that explicitly two-dimensional treatments might be important for understanding bath gas mixing effects, as recently explored by Lei and Burke.[79,80]

The trends in Fig. 4 are further quantified by considering $k_0(E,J)$ apart from $x_0(E,J)$. Cuts through $k_0(E,J)$ for three kinetically-relevant initial rotational states are shown in Fig. 5(a) for M = Ar, N_2, CO_2, and H_2O at 1000 K. (Results for M = NH_3 were found to be similar to those for M = H_2O and are not shown.) Significant reactivity is shown to occur only very close to threshold even for the strongest bath, M = H_2O, with $k_0(E,J)$ decreasing by an order of magnitude just ~300 cm^{-1} below threshold.

In every case, the curves show a narrow energy range very close to threshold where $k_0(E,J)$ declines rapidly with decreasing initial energy as well as a long tail with relatively less initial-state

dependence. The stronger baths have more prominent tails, and these differences can be seen more clearly in Fig. 5(b) in which the results in Fig. 5(a) have been normalized as in eqn 4. The normalization constants are compared with Lennard–Jones collision rates in the figure, and they are shown to be ~20% larger for the weaker baths and 2–3 times larger for the stronger baths. This normalization procedure provides yet another way to define collision rate constants, and we emphasize that it is just as arbitrary as any other. Nonetheless, it lets us develop an intuition regarding the relative likelihood of an activating collision as a function of the initial state of the reactant.

The resulting curves in Fig. 5(b) can be interpreted as state-selected per-collision activation probabilities (eqn 5). We see that for initial states in the "long tail" of the stronger baths, ~10% of collisions are reactive for *both* M = H_2O and CO_2 and that differences in the overall rates for these two baths arise instead from differences in the number of collisions per time, i.e., differences in Z. Observed differences in F might suggest different energy transfer mechanisms, whereas collisional differences in Z are simpler to explain.

Finally, Fig. 5(c) shows microcanonical bath gas efficiencies relative to Ar, again as a function of initial state. The values of $k_0(E,J)$ for the two weak baths, Ar and N_2, show a very similar energy-dependence and a negligible rotational state dependence, and as a result the relative microcanonical collision efficiencies are close to the thermal ones for these baths. In contrast, there is significant initial state dependence for the stronger baths. For M = CO_2, NH_3, and H_2O, the relative values of $k_0(E,J)$ vary by a factor of two or more with initial state, even over the narrow energy range shown in Fig. 5. The relative thermal values necessarily pass through the microcanonical curves near kinetically relevant initial states, as the thermal properties are weighted averages of the underlying microcanonical ones (eqn 2).

IV. Conclusions

The main goal of this work was to demonstrate that pressure-dependent kinetics can be predicted with high accuracy, both for weak atomic and diatomic colliders and for stronger polyatomic colliders including water. By comparing with available experimental results for CH_4 (+M) and HO_2(+M) and with measured relative collision efficiencies for a few other systems, we quantified the expected accuracy of our approach to be better than ~25%, rivaling the accuracy of kinetics experiment in many cases.

A brief presentation of microcanonical rate constants was given, with the goal of rationalizing trends and providing mechanistic insight. Most notably, perhaps, relative microcanonical collision efficiencies were shown to vary significantly as a function of the initial state of the reactant. It is important to emphasize just how surprising the magnitude of this variation is. Notice in Fig. 5(c) that the relative value of $k_{0,H2O}(E,J)/k_{0,Ar}(E,J)$ equals 5 for initial states close to threshold but equals ~40 for initial states just –750 cm^{-1} (~2 kcal/mol) below threshold! One goal of past trajectory studies was to aid in the development of a useful intuition for explaining differences in observed relative collision efficiencies. Such simple explanations seem unlikely when, as in our example, a change of just 2 kcal/mol out of a total internal energy of ~40 kcal/mol leads to such dramatically different relative outcomes.

In our opinion, it seems unavoidable that a priori strategies are needed for predicting collisional energy transfer and its effect on k_0 and k_p that can be applied alongside advanced treatments for thermochemistry and transition state theory now widely in use. The present computations are not significantly more computationally intensive than high-accuracy methods for thermochemistry or transition state theory. We hope that advanced treatments for predicting

collisional energy transfer and pressure-dependent kinetics will find more widespread use such that *both* contributions to unimolecular reactivity central to Lindeman and Hinshelwood's celebrated advance can be treated on equal footing.

Acknowledgements

This work was supported by the U. S. Department of Energy, Office of Basic Energy Sciences, Division of Chemical Sciences, Geosciences, and Biosciences through Argonne National Laboratory. Argonne is a U. S. Department of Energy laboratory managed by UChicago Argonne, LLC, under Contract Number DE-AC02-06CH11357. We gratefully acknowledge computing resources provided by Bebop, a high-performance computing cluster operated by the Laboratory Computing Resource Center at Argonne National Laboratory.

Table 1. Predicted and experimental thermal collision efficiencies relative to Ar

System	300 K	1000 K	2000 K
CH_4 (+M)			
He:Ar	1.01	1.70	2.56
N_2:Ar	1.02	1.10	1.28
O_2:Ar	1.09	1.19	1.33
H_2:Ar	2.29	3.31	4.09
CO_2:Ar	1.64	1.65	1.77
CH_4:Ar	2.98	4.66	5.11
H_2O:Ar	4.17	6.19	6.96
HO_2 (+M)			
He:Ar	0.90 (0.82)[a]	1.17	1.34
N_2:Ar	1.71 (1.95)[a]	1.58 (1.79)[b]	1.20 (1.38)[c]
H_2:Ar	3.69 (2.52)[a]	3.07	1.71
CO_2:Ar	13.7	8.94 (4.29)[b]	3.03 (5.0)[c]
NH_3:Ar	20.4	17.9	18.7
H_2O:Ar	23.3 (22.7)[a]	22.2 (18.9)[b]	21.3 (23.0)[c]
H_2O_2 (+M)			
N_2:Ar	1.50	1.58 (1.49)[d]	1.63
CO_2:Ar	5.22	4.14 (1.85)[d]	3.27
H_2O_2:Ar	6.83	12.0 (6.42)[d]	16.3
H_2O:Ar	5.51	10.2 (9.85)[d]	13.3
H_2O (+M)			
N_2:Ar	2.51	1.62	1.20
H_2O:Ar	8.97 (6.7)[e]	8.55 (9.3)[e]	8.75 (14.6)[e]
NH_3 (+M)			
N_2:Ar	3.15[f]	2.47	2.25
O_2:Ar	1.55	1.48	1.70
CO_2:Ar	11.2[f]	13.4	14.3
NH_3:Ar	13.9	20.0	22.2
CH_4:Ar	9.94[f]	13.3	14.3
H_2O:Ar	14.0	23.6	27.9
N_2H_4 (+M)			
N_2:Ar	2.00 (2.5)[g] (1.3)[h]	1.69	1.43
O_2:Ar	1.22	1.17	1.14
NH_3:Ar	5.86 (10)[g] (5.2)[h]	8.25	8.60
H_2O:Ar	5.60	7.98	8.19
HNO (+M)			
N_2:Ar	1.61	1.71	1.59
H_2O:Ar	6.42	8.15	9.09
HCN (+M)			
N_2:Ar	1.05	1.26	1.47
H_2O:Ar	4.24	4.87	5.56

[a]Michael et al.[69]; [b]Ashman and Haynes[70] at 750–900 K; [c]Shao et al.[68] at 1500 K; [d]Hong et al.[72]; [e]Srinivasan and Michael[73]; [f]N_2:CH_4:CO_2 = 1 : 3.15 : 3.54 at 300 K, which agrees well with the relative experimental values of 1 : 2.60 : 2.83 of Macdonald and co-workers.[75–77] [g]Khe at al.[78] [h]Macdonald and co-workers.[75–77]

References

[1] F. A. Lindemann, S. Arrhenius, I. Langmuir, N. R. Dhar, J. Perrin, and W. C. McC. Lewis, Discussion on "The Radiation Theory of Chemical Action." *Trans. Faraday Soc.* 1922, **17**, 598−606.

[2] C. N. Hinshelwood, On the Theory of Unimolecular Reactions. *Proc. R. Soc. London, Ser. A* 1926, **113**, 230−233.

[3] O. K. Rice and H. C. Ramsperger, Theories of Unimolecular Gas Reactions at Low Pressures, *J. Am. Chem. Soc.* 1927, **49**, 1617–1629.

[4] L. S. Kassel, Studies in Homogeneous Gas Reactions I, *J. Phys. Chem.* 1928, **32**, 225–242.

[5] R. A. Marcus, Unimolecular Dissociations and Free Radical Recombination Reactions, *J. Chem. Phys.* 1952, **20**, 359–364.

[6] T. Baer and W. L. Hase, *Unimolecular Reaction Dynamics: Theory and Experiments* (Oxford University Press, New York, 1996).

[7] D. G. Truhlar, B. C. Garrett, and S. J. Klippenstein, Current Status of Transition State Theory. *J. Phys. Chem.* 1996, **100**, 12771–12800.

[8] L. B. Harding, S. J. Klippenstein, and A. W. Jasper, Ab Initio Methods for Reactive Potential Energy Surfaces. *Phys. Chem. Chem. Phys.* 2007, **9**, 4055-4070.

[9] M. J. Pilling, Reactions of Hydrocarbon Radicals and Biradicals. *J. Phys. Chem. A* 2013, **117**, 3697–3717.

[10] S. J. Klippenstein, From Theoretical Reaction Dynamics to Chemical Modeling of Combustion. *Proc. Comb. Inst*. 2017, **36**, 77–111.

[11] J. R. Barker, Direct Measurements of Energy-Transfer Involving Large Molecules in the Electronic Ground State. *J. Phys. Chem.* 1984, **88**, 11–18.

[12] H. Hippler, L. Lindemann, and J. Troe, Collisional Energy Transfer of Vibrationally Highly Excited Molecules. V. UV Absorption Study of Azulene. *J. Chem. Phys.* 1985, **83**, 3906–3912.

[13] M. L. Yerram, J. D. Brenner, K. D. King, and J. R. Barker, Collisional Deactivation of Highly Vibrationally Excited Benzene Pumped at 248 nm. *J. Phys. Chem.* 1990, **94**, 6341–6350.

[14] C. R. Bieler, A. Sanov, C. Capellos, and H. Reisler, Molecular Beams Studies of the Dissociation of Highly Excited NO_2 Induced by Molecular Colliders. *J. Phys. Chem.* 1996, **100**, 3882–3887.

[15] G. W. Flynn, C. S. Parmenter, and A. M. Wodtke, Vibrational Energy Transfer. *J. Phys. Chem.* 1996, **100**, 12817–12838.

[16] T. Lenzer, K. Luther, K. Reihs, and A. C. Symonds, Collisional Energy Transfer Probabilities of Highly Excited Molecules from Kinetically Controlled Selective Ionization (KCSI). II. The Collisional Relaxation of Toluene: $P(E',E)$ and Moments of Energy Transfer for Energies up to 50000 cm^{-1}. *J. Chem. Phys.* 2000, **112**, 4090–4110.

[17] C. L. Liu, H. C. Hsu, J. J. Lyu, and C. K. Ni, Energy Transfer of Highly Vibrationally Excited Azulene: Collisions Between Azulene and Krypton. *J. Chem. Phys.* 2006, **124**, 054302.

[18] T. Lenzer and K. Luther, On the Accuracy of Collisional Energy Transfer Parameters for Reaction Kinetics Applications: Detailed Evaluation of Data from Direct Experiments. *Phys. Chem. Chem. Phys.* 2004, **4**, 995–959.

[19] J. Du, N. A. Sassin, D. K. Havey, K. Hsu, and A. S. Mullin, Full State-Resolved Energy Gain Profiles of CO_2 from Collisions with Highly Vibrationally Excited Molecules. II. Energy-Dependent Pyrazine (E = 32700 and 37900 cm^{-1}) Relaxation. *J. Phys. Chem. A* 2013, **46**, 12104–12115.

[20] J. D. Steill, A. W. Jasper, and D. W. Chandler, Determination of the Collisional Energy Transfer Distribution Responsible for the Collision-Induced Dissociation of NO_2 with Ar. *Chem. Phys. Lett.* 2015, **636**, 1–14.

[21] K. D. King and J. R. Barker, In *Unimolecular Kinetics: Parts 2 and 3: Collisional Energy Transfer and the Master Equation*, edited by S. H. Robertson, (Elsevier, 2019), pp. 3–62.

[22] J. Troe, Theory of Thermal Unimolecular Reactions at Low-Pressures. 1. Solutions of the Master Equation. *J. Chem. Phys.* 1977, **66**, 4745–4757.

[23] A. W. Jasper, Microcanonical rate constants for unimolecular reactions in the low-pressure limit. *J. Chem. Phys. A* 2020, **124**, 1205–1226.

[24] D. L. Bunker and S. A. Jayich, Trajectory Studies of Energy Transfer: CH_3NC with He, Xe, H_2, and N_2. *Chem. Phys.* 1976, **13**, 129–134.

[25] N. J. Brown and J. A. Miller, Collisional Energy-Transfer in the Low-Pressure-Limit Unimolecular Dissociation of HO_2. *J. Chem. Phys.* 1984, **80**, 5568–5580.

[26] X. Hu and W. L. Hase, Effect of Anharmonicity on Intermolecular Energy-Transfer from Highly Vibrationally Excited Molecules. *J. Phys. Chem.* 1988, **92**, 4040–4064.

[27] G. Lendvay and G. C. Schatz, Observation of Highly Energetic Collisions in Classical Trajectory Studies of Collisional Energy Transfer. *J. Phys. Chem.* 1990, **94**, 8864–8866.

[28] K. F. Lim and R. G. Gilbert, Calculation of Collisional-Energy-Transfer Rates in Highly Excited Molecules. *J. Phys. Chem.* 1990, **94**, 72–77.

[29] R. G. Gilbert, Theory of Collisional Energy Transfer of Highly Excited Molecules. *Int. Rev. Phys. Chem.* 1991, **10**, 319–347.

[30] D. L. Clarke, I. Oref, R. G. Gilbert, and K. F. Lim, Collisional Energy Transfer in Highly Excited Molecules: Calculations of the Dependence on Temperature and Internal, Rotational, and Translational Energy. *J. Chem. Phys.* 1992, **96**, 5983–5998.

[31] T. Lenzer, K. Luther, J Troe, R. G. Gilbert, and K. F. Lim, Trajectory Simulations of Collisional Energy-Transfer in Highly Excited Benzene and Hexafluorobenzene. *J. Chem. Phys.* 1995, **103**, 626–641.

[32] J. R. Barker, L. M. Yoder, and K. D. King, Vibrational Energy Transfer Modeling of Nonequilibrium Polyatomic Reaction Systems. *J. Phys. Chem. A* 2001, **105**, 796–809.

[33] I. Oref, Collisional Energy Transfer in Polyatomic Molecules in the Gas Phase. *Israel J. Chem.* 2007, **47**, 205–214.

[34] R. Conte, P. L. Houston, and J. M. Bowman, Classical Trajectory Study of Energy Transfer in Collisions of Highly Excited Allyl Radical with Argon. *J. Phys. Chem. A* 2013, **117**, 14028–14041.

[35] J. W. Perry and A. F. Wagner, Pressure Effects on the Relaxation of an Excited Hydrogen Peroxyl Radical in an Argon Bath, *J. Phys. Chem. A* 2017, **36**, 229–236.

[36] A. K. Paul, N. A. West, J. D. Winner, R. D. W. Bowersox, S. W. North, and W. L. Hase, Non-statistical Intermolecular Energy Transfer from Vibrationally Excited Benzene in a Mixed Nitrogen-Benzene Bath. *J. Chem. Phys.* 2018, **149**, 134101.

[37] H. Wang, K. Wen, X. You, Q. Mao, K. H. Luo, M. J. Pilling, and S. H. Robertson, Energy Transfer in Intermolecular Collisions of Polycyclic Aromatic Hydrocarbons with Bath Gases He and Ar. *J. Chem. Phys.* 2019, **151**, 044301.

[38] R. M. Zhang, X. F. Xu, and D. G. Truhlar Energy Dependence of Ensemble-Averaged Energy Transfer Moments and Its Effect on Competing Decomposition Reactions**,** *J. Phys. Chem. A* 2021, **125**, 6303–6313.

[39] A. W. Jasper and J. A. Miller, Collisional Energy Transfer in Unimolecular Reactions: Direct Classical Trajectories for $CH_4 \rightarrow CH_3 + H$ in Helium. *J. Phys. Chem. A* 2009, **113**, 5612–5619.

[40] A. W. Jasper and J. A. Miller, Theoretical Unimolecular Kinetics for $CH_4 + M \rightarrow CH_3 + H + M$ in Eight Baths, M = He, Ne, Ar, Kr, H_2, CO, N_2, and CH_4, *J. Phys. Chem. A*. 2011, **115**, 6438–6455.

[41] A. W. Jasper, J. A. Miller, and S. J. Klippenstein, The Collision Efficiency of Water in the Unimolecular Reaction $CH_4 (+ H_2O) \rightarrow CH_3 + H (+ H_2O)$: One-Dimensional and Two-Dimensional Solutions of the Low-Pressure-Limit Master Equation, *J. Phys. Chem. A*. 2013, **117**, 12243–12255.

[42] A. W. Jasper, C. M. Oana, and J. A. Miller, "Third-Body" Collision Efficiencies for Combustion Modeling: Hydrocarbons in Atomic and Diatomic Baths. *Proc. Combust. Inst.* 2015, **35**, 197–204.

[43] A. W. Jasper, "Third-body" collision parameters for hydrocarbons, alcohols, and peroxides and an effective internal rotor approach for estimating them. *Int. J. Chem. Kinet.* 2020, **52**, 387–402 (2020).

[44] J. R. Barker and R. E. Weston, Collisional Energy Transfer Probability Densities $P(E,JE',J')$ for Monatomics Colliding with Large Molecules. *J. Phys. Chem. A* 2010, **114**, 10619–10633.

[45] G. Lendvay, In *Unimolecular Kinetics: Parts 2 and 3: Collisional Energy Transfer and the Master Equation, Vol. 43*, edited by S. H. Robertson, (Elsevier, 2019), pp. 110–272.

[46] D. G. Truhlar, and J.T. Muckerman, "Reactive Scattering Cross Sections: Quasiclassical and Semiclassical Methods," in *Atom-Molecule Collision Theory*: *A Guide for the Experimentalist*, edited by R. B. Bernstein, (Plenum Press, New York, 1979), pp. 505–566.

[47] H. C. Andersen, Molecular Dynamics Simulations at Constant Pressure and/or Temperature. *J. Chem. Phys.* 1980, **72**, 2348–2393.

[48] D. G. Truhlar and J. T. Muckerman, in "Atom-Molecule Collision Theory: A Guide for the Experimentalist," edited by R. D. Bernstein (Plenum, New York, 1979), pp. 505–566.

[49] L. M. Raff and D. L. Thompson, in "Theory of Chemical Reaction Dynamics, Vol. 3," edited by M. Baer (CRC Press, Boca Raton, 1985), pp. 1–121.

[50] A. W. Jasper and J. A. Miller, Lennard-Jones Parameters for Combustion and Chemical Kinetics Modeling from Full-Dimensional Intermolecular Potentials. *Combust. Flame* 2013, **161**, 101–110.

[51] B. J. Braams and J. M. Bowman, Permutationally Invariant Potential Energy Surfaces in High Dimensionality, *Int. Rev. Phys. Chem.* 2009, **28**, 577–606.

[52] A. W. Jasper and M. J. Davis, Parameterization Strategies for Intermolecular Potentials for Predicting Trajectory-Based Collision Parameters. *J. Phys. Chem. A* 2019, **123**, 3464–3480.

[53] D. R. Moberg and A. W. Jasper, Permutationally invariant polynomial expansions with unrestricted complexity. *J. Chem. Theory Comput.* 2021, **17**, 5440–5455 .

[54] NIST Computational Chemistry Comparison and Benchmark Database, NIST Standard Reference Database Number 101, Release 21, August 2020, Editor: R. D. Johnson III, http://cccbdb.nist.gov/

[55] S. J. Jeffrey, K. E. Gates, and S. C. Smith, Full Iterative Solution of the Two-Dimensional

Master Equation for Thermal Unimolecular Reactions. *J. Phys. Chem.* 1996, **100**, 7090–7096.

[56] S. H. Roberston, M. J. Pilling, K. E. Gates, and S. C. Smith, Application of Inverse Iteration to 2-Dimensional Master Equations. *J. Comp. Chem.* 1997, **18**, 1004–1010.

[57] A. W. Jasper, K. M. Pelzer, J. A. Miller, E. Kamarchik, L. B. Harding, and S. J. Klippenstein, Predictive A Priori Pressure-Dependent Kinetics. *Science* 2014, **346**, 1212–1215.

[58] A. S. Hansen, T. Bhagde, K. B. Moore III, D. R. Moberg, A. W. Jasper, Y. Georgievskii, M. F. Vansco, S. J. Klippenstein, and M. I. Lester, Watching a hydroperoxyalkyl radical (•QOOH) dissociate. *Science* 2021, **373**, 679-682.

[59] S. J. Klippenstein, A bond length reaction coordinate for unimolecular reactions. II. Microcanonical and canonical implementations with application to the dissociation of NCNO. J. Chem. Phys. 1991, **94**, 6469–6482.

[60] L. B. Harding, Y. Georgievskii, and S. J. Klippenstein, Predictive theory for hydrogen atom-hydrocarbon radical association kinetics. *J. Phys. Chem. A* 2005, **109**, 4646–4656.

[61] E. Kamarchik and A. W. Jasper, Anharmonic state counts and partition functions for molecules via classical phase space integrals in curvilinear coordinates. *J. Chem. Phys.* 2013, **138**, 194109.

[62] A. W. Jasper, L. B. Harding, C. Knight, and Y. Georgievskii, Anharmonic rovibrational partition functions at high temperatures: Tests of reduced-dimensional models for systems with up to three fluxional modes. *J. Phys. Chem. A* **123**, 6210–6228 (2019).

[63] N. J. Labbe, A. W. Jasper, J. A. Miller, S. J. Klippenstein, B. Ruscic, and R., Sivaramakrishnan, in preparation. See also N. J. Labbe, A. W. Jasper, J. A. Miller, S. J. Klippenstein, B. Ruscic, and R. Sivaramakrishnan, High Accuracy Thermochemical Kinetics for H + CH_3 (+M) ⇄ CH_4 (+M), Paper 1A01, 10th US National Combustion Meeting, MD, 2017.

[64] C. J. Chen, M. H. Back, A. R. Back, The Thermal Decomposition of Methane. I. Kinetics of the Primary Decomposition to $C_2H6 + H_2$; Rate Constant for the Homogeneous Unimolecular Dissociation of Methane and its Pressure Dependence. *Can. J. Chem.* 1975, **53**, 3580–3590.

[65] R. W. Barnes, G. L. Pratt, and S. W. Wood, Pressure dependence of methane dissociation. *J. Chem. Soc. Faraday Trans. 2* 1989, **85**, 229–238.

[66] D. F. Davidson, E. L. Petersen, M. Röhrig, R. K. Hanson, C. T. Bowman, Measurement of the rate coefficient of $H+O_2+M \rightarrow HO_2+M$ for M=Ar and N_2 at high pressures. *Proc. Combust. Inst.* 1996, **26**, 481–488.

[67] R. W. Bates , D. M. Golden, R. K. Hanson, C. T. Bowman, Experimental study and modeling of the reaction $H + O_2 + M \rightarrow HO_2 + M$ (M = Ar, N_2 , H_2O) at elevated pressures and temperatures between 1050 and 1250 K. *Phys. Chem. Chem. Phys.* 2001, **3**, 2337–2342.

[68] J. Shao, R. Choudhary, A.Susa, D. F. Davidson, and R. K. Hanson, Shock Tube Study of the Rate Constants for $H + O_2 + M \rightarrow HO_2 + M$ (M = Ar, H_2O, CO_2, N_2) at Elevated Pressures. *Proc. Combust. Inst.* 2019, **37**, 145–152.

[69] J. V. Michael, M.-C. Su, J. W. Sutherland, J. J. Carroll, and A. F. Wagner, Rate Constants For $H + O_2 + M \rightarrow HO_2 + M$ in Seven Bath Gases. *J. Phys. Chem. A*, 2002, **106**, 5297–5313.

[70] P. J. Ashman and B. S. Haynes, Rate Coefficient of $H + O_2 + M \rightarrow HO_2 + M$ (M = H_2O, N_2, Ar, CO_2). *Proc. Combust. Inst.* 1998, **27**, 185–191.

[71] A. Matsugi, Modeling Third-Body Effects in the Thermal Decomposition of H_2O_2, *Combust. Flame* 2021, **225**, 444–452.

[72] Z. Hong, A. Farooq, E. A. Barbour, D. F. Davidson, and R. K. Hanson, Hydrogen Peroxide Decomposition Rate: A Shock Tube Study Using Tunable Laser Absorption of H_2O near 2.5 μm. *J. Phys. Chem. A* 2009, **113**, 12919–12925.

[73] N. K. Srinivasan and J. V. Michael, The Thermal Decomposition of Water. *Int. J. Chem. Kinet.* 2006, **38**, 211–219.

[74] P. Glarborg, H. Hashemi, S. Cheskis, and A. W. Jasper, On the rate constant for NH_2+HO_2 and third body collision efficiencies for NH_2+H(+M) and NH_2+NH_2(+M). *J. Phys. Chem. A* 2021, **125**, 1505–1516.

[75] G. Altinay and R. G. Macdonald. Determination of the Rate Constants for the $NH_2(X^2B_1)$ + $NH_2(X^2B_1)$ Recombination Reaction with Collision Partners He, Ne, Ar, and N_2 at Low Pressures and 296 K. Part 1. *J. Phys. Chem. A*, 2012, **116**, 1353–1367.

[76] G. Altinay and R. G. Macdonald. Determination of the Rate Constants for the $NH_2(X^2B_1)$ + $NH_2(X^2B_1)$ and $NH_2(X^2B_1)$ + H Recombination Reactions with Collision Partners CH_4, C_2H_6, CO_2, CF_4, and SF_6 at Low Pressures and 296 K. Part 2. *J. Phys. Chem. A*, 2012, **116**, 2161–2176.

[77] G. Altinay and R. G. Macdonald. Determination of the rate constants for the $NH_2(X^2B_1)$ + $NH_2(X^2B_1)$ and $NH_2(X^2B_1)$ + H recombination reactions in N_2 as a function of temperature and pressure. *J. Phys. Chem. A*, 2015, **119**, 7593–7610.

[78] P. V. Khe, J. C. Soulignac, and R. Lesclaux. Pressure and temperature dependence of amino radical recombination rate constant. *J. Phys. Chem.*, 1977, **81**, 210–214.

[79] L. Lei and M. P. Burke, Bath Gas Mixture Effects on Multichannel Reactions: Insights and Representations for Systems beyond Single-Channel Reactions. *J. Phys. Chem. A*, 2019, **123**, 631–649.

[80] L. Lei and M. P. Burke, Mixture rules and falloff are now major uncertainties in experimentally derived rate parameters for H + O_2 (+M) HO_2 (+M). *Combust. Flame*, 2020, **213**, 467–474.

Figure 1

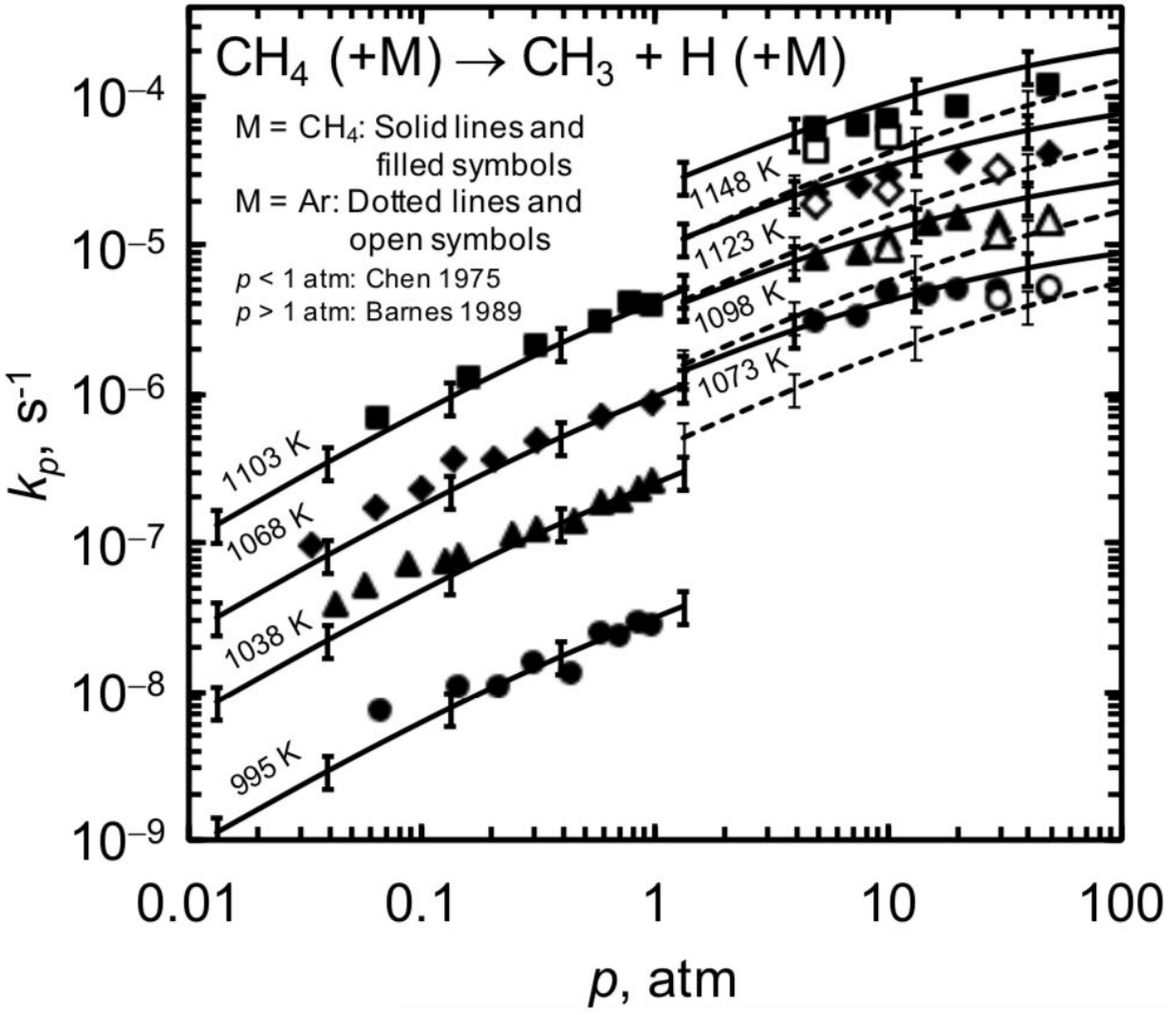

Fig. 1. Predicted (lines) and experimental (symbols) pressure-dependent thermal rate constants k_p for CH_4 (+M), M = Ar and CH_4 around 1000 K. The lower-pressure measurements are from Chen et al.,[64] and the higher-pressure measurements are from Barnes et al.[65]

Figure 2

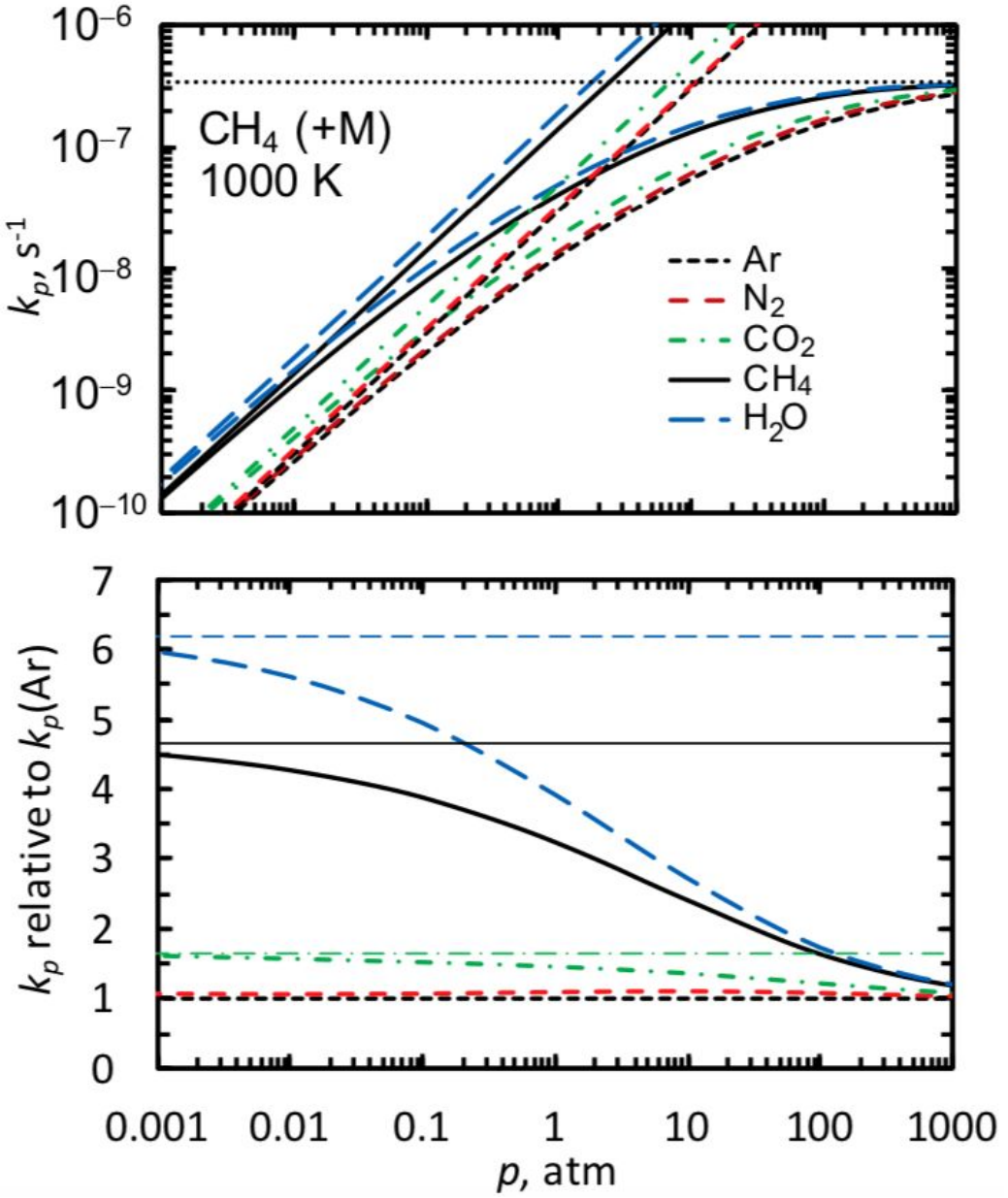

Fig. 2. The upper panel shows predicted pressure-dependent thermal rate constants k_p for CH_4 (+M) in five baths at 1000 K. The horizontal dotted line indicates the calculated high-pressure limit, and the other straight lines show low-pressure limit rate constants multiplied by the number density of the bath gas, $k_0 n_M$. The lower panel shows the relative values of k_p from the upper panel, and the horizontal lines indicate the relative values of k_0.

Figure 3

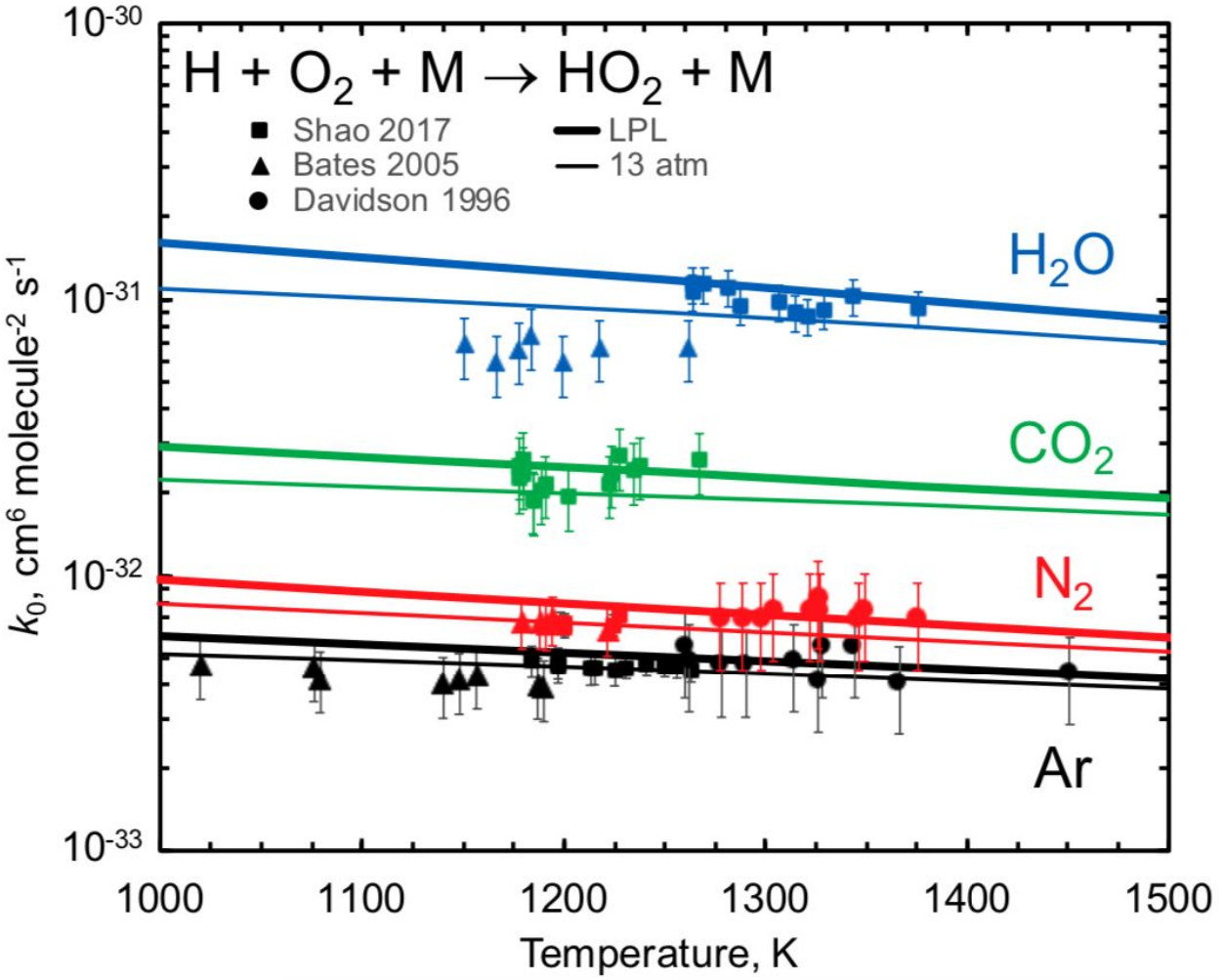

Fig. 3. Predicted low-pressure-limit (LPL) thermal rate constants k_0 for H + O_2 + M in four baths from 1000–1500 K. The thicker lines show the calculated LPLs, and the thinner lines show the calculated rate constants at 13 atm. The predictions are compared with results from three experimental studies.[66–68] Note that for M = N_2, the red squares and red triangles overlap and are difficult to distinguish.

Figure 4

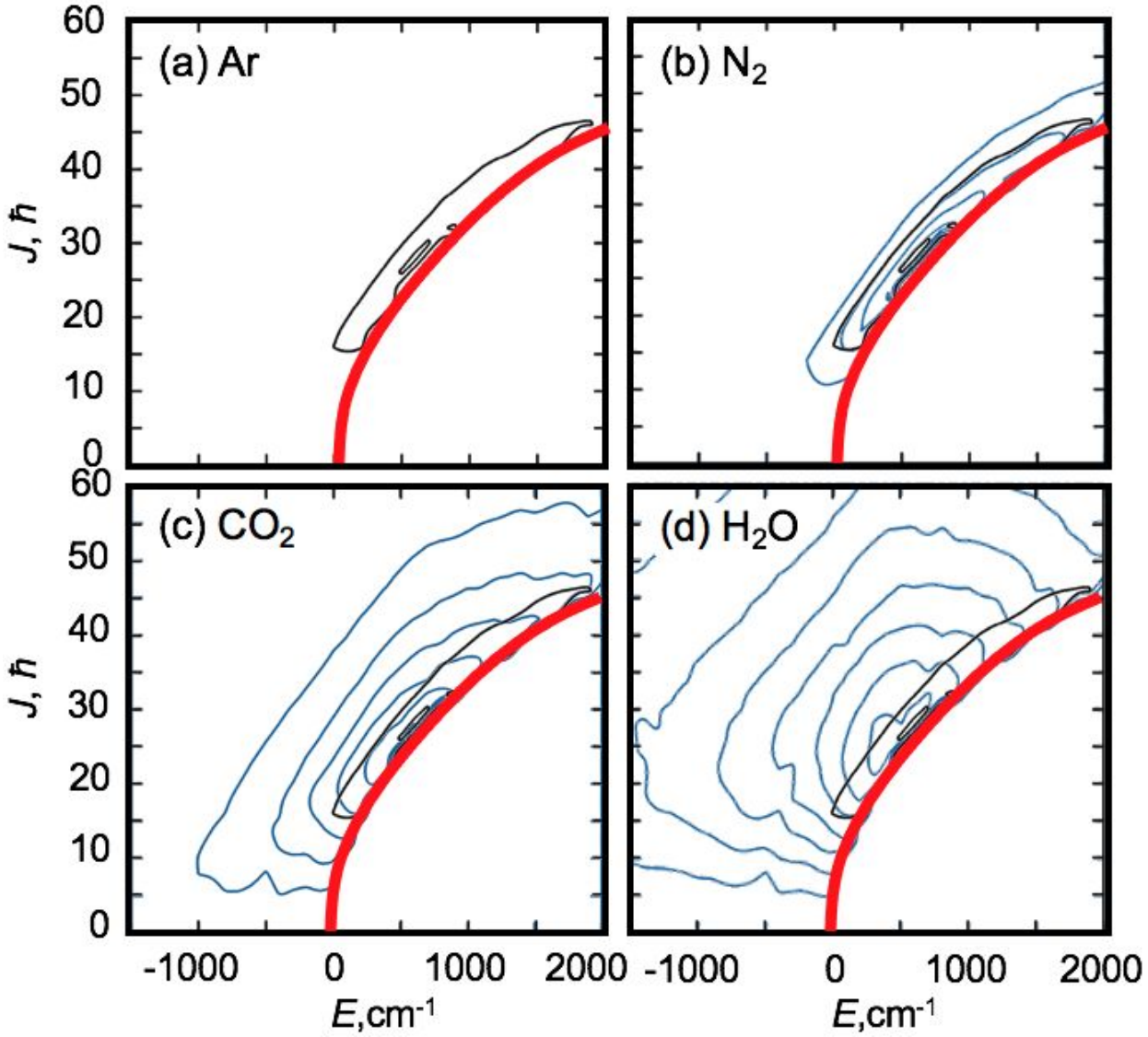

Fig. 4. Contour plots of k_0x_0, the state-selected contribution to the low-pressure-limit thermal rate constant, for HO_2 (+M) at 1000 K. The plot for M = Ar (black) is overlaid on the plots for the other baths (blue). The red line shows E_J, the rotational-state-dependent dissociation threshold. A consistent set of evenly spaced contour lines were used in all four panels, with 2, 4, 5, and 7 contours appearing for M = Ar, N_2, CO_2, and H_2O, respectively.

Figure 5

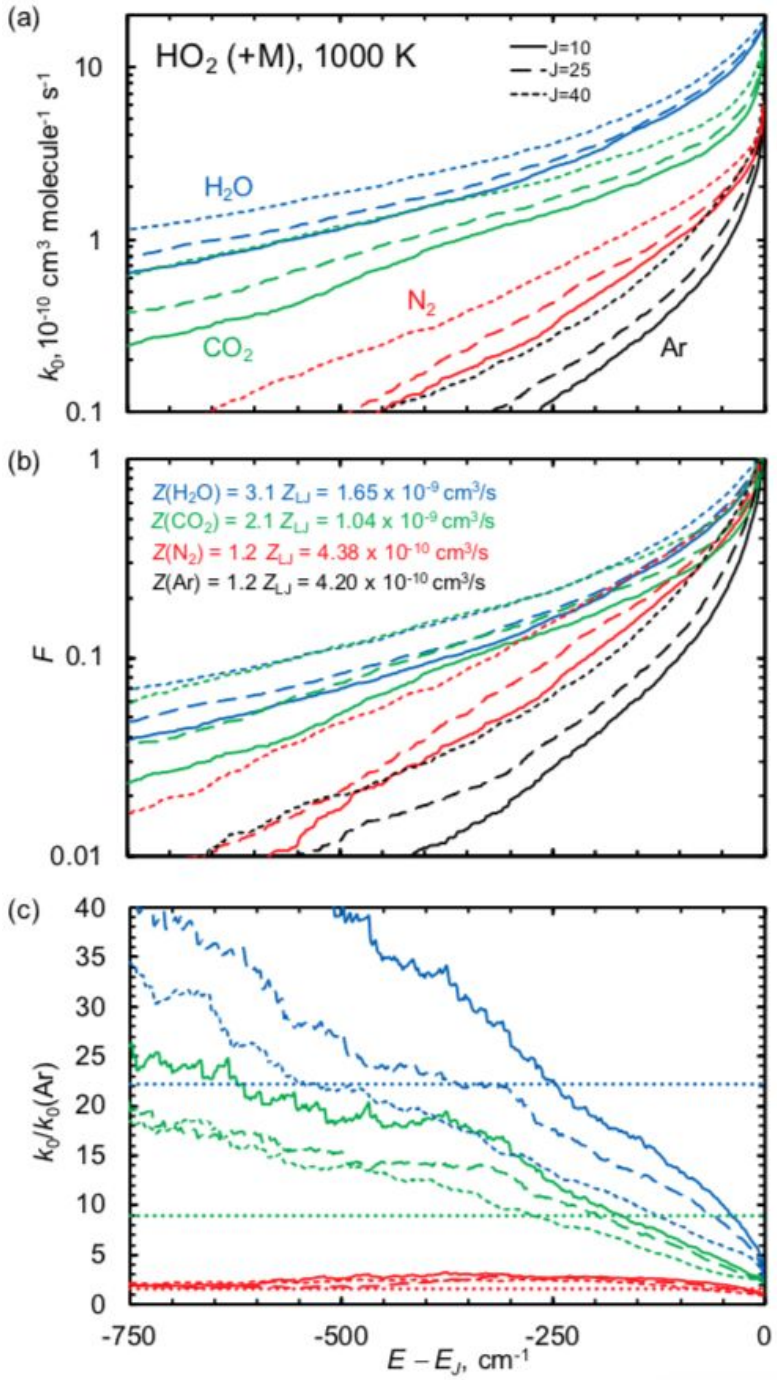

Fig. 5. (a) Microcanonical rate constants $k_0(E,J)$ for HO_2 (+M), J = 10, 25, and 40 $\hbar$, and M = Ar, N_2, CO_2, and H_2O shown relative to the rotationally-adiabatic dissociation threshold E_J. (b) Collisional activation probabilities $F(E,J) = k_0(E,J)/Z$ scaled to the collision rates Z given in the figure and described in the text. (c) Microcanonical collision efficiencies relative to those for Ar. The horizontal lines show the relative thermal collision efficiencies from Table 1.